Numerical study to understand thermo-mechanical effects on a composite-aluminium hybrid bolted joint

A. Sasikumar[a,*], J.M. Guerrero[a], A. Quintanas-Corominas[a,**], J. Costa[a]

[a] *AMADE, Polytechnic School, University of Girona, Campus Montilivi s/n, 17073 Girona, Spain*

Abstract

Hybrid bolted joints, where carbon fiber reinforced polymers and metallic plates are clamped using bolts, are widely used in aircraft structures. During operation, aircraft experience extreme temperatures that can adversely affect the response of an hybrid joint. On account of the lack of understanding on this aspect, we analyzed a representative carbon-aluminum single lap shear bolted joint using a 3D numerical model. A parametric study varying the temperature, friction coefficient, bolt clamping force, bolt-hole clearance, and thickness of the metallic plate, provided insight into their effect on the stiffness stages of the mechanical response of the joint, as well as the contact evolution among the different elements. Bolt-hole clearance was one of the parameters that most influenced the joint stiffness and bolt bending. Temperature excursions induced sliding between plates and significantly altered the clamping load of the bolt, i.e., a 40% reduction and an 18% increase for a negative and positive thermal jumps, respectively. This clamping load variation entails undesirable bolt loosening or even yielding. Therefore, this work sheds light on the detrimental effects of temperature on hybrid joints, thus providing background for a safer structural design.

Keywords: Hybrid bolted joints, Thermal effect, Aircraft structure, Joint response

1. Introduction

Bolted joints are extensively used in aeronautical structures due to their efficiency in transferring load and ease of service and repair[1; 2]. Understanding the mechanical response of a bolted joint is complex because of the contact interaction of several parts and the stress concentrations at the bolt hole. Despite the considerable amount of published work [3; 4], the design of bolted joints is still a challenging task, particularly when environmental factors need to be accounted for.

In the last decades, aircraft industries have increased the use of Carbon Fiber Reinforced Polymer (CFRP) materials, but at the same time have maintained metallic components (aluminium, titanium) in the primary structure of the aircraft. This has led to hybrid joint assemblies routinely found in structural components such as the wings, empennage or fuselage. For example, the Airbus A380 utilizes lightweight carbon fiber skins connected to aluminium ribs in its wings. However, within a

*Corresponding Author : Aravind Sasikumar
**Current Address: Barcelona Supercomputing Center, c/ Jordi Girona 31, 08034, Barcelona, Spain
Email address: aravind.sasikumar@udg.edu (A. Sasikumar)

few years of service, cracks have been found on the rib feet which had originated from the rib-to-skin panel attachment holes. In addition, cracks were found at the vertical web of the rib feet [5]. The Airworthiness Directive issued by the FAA, stated that this condition could potentially affect the structural integrity of the aircraft. Preliminary investigations accounted this to the high stresses at the joint between dissimilar materials and also to differential response to extreme temperatures [6]. This critical situation evidences that there is still a need to adequately understand the response of hybrid bolted joints under different operating conditions.

An aircraft experiences temperatures in the range of -30°C to -55°C at cruising altitudes, and between 45°C to 50°C when landed, depending on the destination airport. The difference in the thermal expansion coefficient of carbon and aluminum induces differential expansion/contraction, leading to difficult-to-predict thermal stresses and uneven responses in the bolted plates, as well as significant variations in the bolt clamping forces. Studies on the thermal load effects on dissimilar material bolted joints are barely touched on the literature [7]. That said, Coman et al. [7] experimentally and numerically studied the temperature effect damage initiation and propagation have on a hybrid bolted joint using strain gauge measurements and a 3D finite element model with damage. Other researchers [8–10] concentrated on the dependence of the bearing strength and damage modes of bolted joints at different temperatures. However, a lack of understanding still remains as to how thermal loads affect the bolts' preload, the sliding of the dissimilar parts and the evolution of the contact forces between the different parts.

Apart from the thermal effects, there are several joint parameters that affect a bolted joint's response [11; 12]. McCarthy et al. [13; 14] experimentally investigated the effect bolt-hole clearance has on the composite-composite bolted joint strength and stiffness and reported a 10% joint stiffness loss due to an increase in the bolt-hole clearance; contrary to the findings reported in [15]. The same authors [16; 17] also numerically studied the bolt-hole clearance effect using 3D finite element analysis and concluded this parameter is crucial in the design of bolted joints. Friction is another important parameter and the least discussed in the literature. The coefficient of friction value varies depending on the material of the joining parts, surface treatment, surface ply orientations in a composite laminate, etc., [18; 19]; all of which potentially affect the response of the joint. The friction coefficient is quite complex to determine experimentally [20]. Regarding the bolt preload, Oskouei et al. [21] studied the variation in the preload clamping force due to applied longitudinal tensile load applied in an aerospace bolted plate. Lv et al. [22] concluded that there was a significant change in the bolt preload when the temperature and the initial preload were varied.

In addition to the experimental tests [23], researchers have used analytical [24–26] and numerical methods [4; 9; 27–33] to predict the behavior of bolted joints. While the former is efficient in the preliminary design stage, the latter is required for detailed understanding and accurate predictions. In the framework of Finite Element (FE) analysis, early researchers used simplified models to economically study bolted joints. Kim et al. [34] investigated different bolt modeling cases such as using 3D solid or beam elements and also compared the results with a no bolt case (where a pretension was directly applied to the washer surface without physically modeling a bolt). They concluded that for accurate responses, it is important to use 3D models that take into account the contact interactions, bolt preload and complex 3D stress states around the bolts. Advances in FE tools have made it possible to virtually study the effect of several parameters on the response, which is quite infeasible experimentally.

This work is set within the framework of an ongoing EU Cleansky 2 project 'INNOHYBOX', developed by the consortium of Dassault Aviation, University of Girona, Eurecat and Sofitec. The global objective of the project is to experimentally and numerically analyze the hybrid wing box of an aircraft under thermo-mechanical loads. The study presented here is a primary investigation performed at a coupon level to understand the bolted joint response. Using a detailed 3D numerical model, we study the thermo-mechanical response of a single lap shear bolted CFRP-aluminium joint with a countersunk fastener by simulating bolt preload, thermal step and followed by a static tensile test. The different stages of the joint response and the evolution of the contact surfaces are discussed, and the contribution of the frictional and normal forces at each stage presented. Further, we perform an exhaustive parametric study to study what the effects of friction coefficient, bolt clamping force, bolt-hole clearance and the thickness of the aluminium plates have. More importantly, we simulate a temperature jump (positive or negative) before the tensile loading and demonstrate the significant effect this has on the bolt clamping load and contact evolution. Finally, to reproduce the conditions of aircraft in service, we simulated a loading-unloading-reloading loop.

2. Methodology

2.1. Numerical model

We developed a detailed 3D numerical model of a Single Lap Shear (SLS) bolted joint in ABAQUS Standard 6.14 [35], using the implicit static solver framework. Fig. 1 illustrates the SLS specimen containing the following parts: i) a CFRP multi-directional laminate made of 60 plies leading to a total thickness of 7.8 mm; ii) an aluminium plate with a thickness of 6 mm; iii) a countersunk fastener made of steel with a shank diameter of 4.78 mm and a countersunk angle of 100° and iv) doubler (CFRP and aluminium) plates placed on either side of the specimen to counteract the moments in an SLS specimen. Table 1 details the different materials used and their corresponding material properties (taken from [36]).

Fig. 1 also depicts the dimensions of the SLS specimen, which are mostly in accordance with the ASTM standard D5961/D5961-M [37]. All the parts were modeled individually and assembled in the

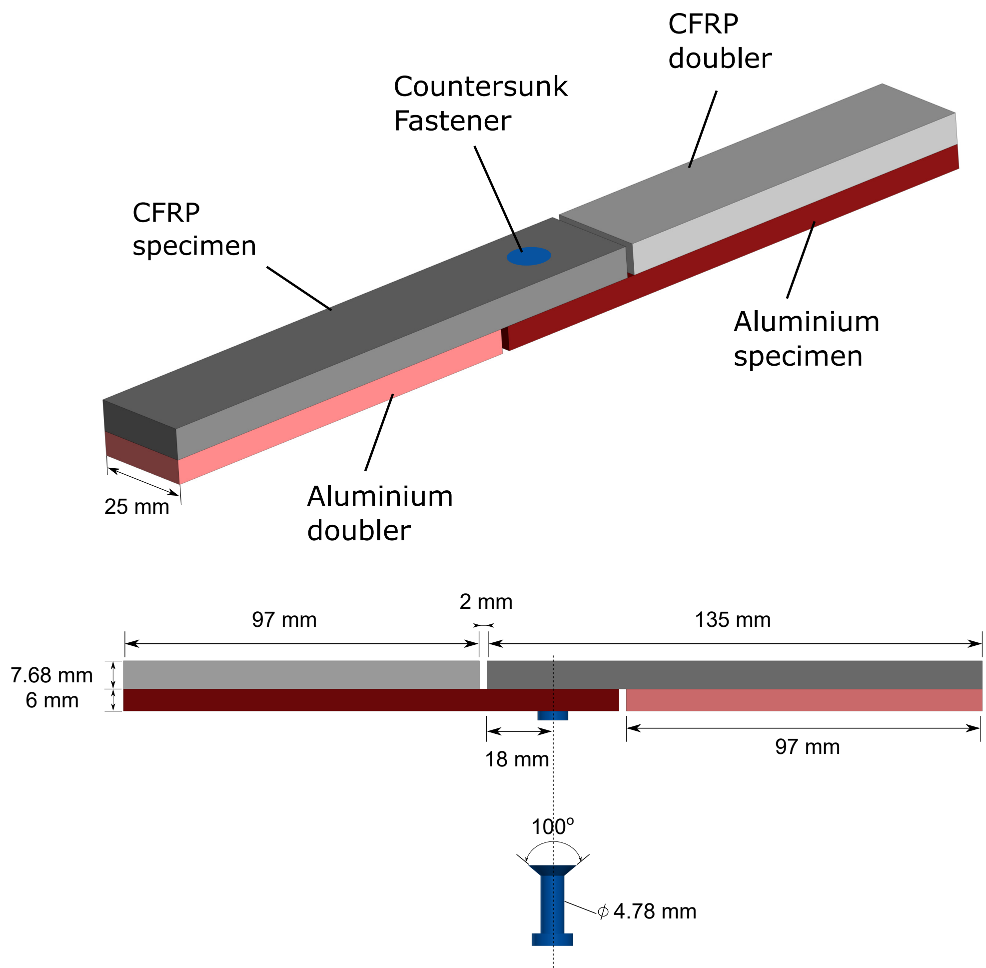

Figure 1: Schematic illustration of the single lap shear bolted joint comprising of CFRP-aluminium plates with a steel countersunk fastener, along with the dimensions of the different parts.

Table 1: Different materials used and the respective material properties (Taken from [36]).

Material	Property	Value
Steel alloy	E [MPa]	21000
	ν [-]	0.3
	α [μm/m°C]	11
	ρ [g/cm^3]	8
Aluminium (Al 2024-O)	E [MPa]	73100
	ν [-]	0.33
	α [μm/m°C]	21.1
	ρ [g/cm^3]	2.7
CFRP (M21 EV/ IMA)	E_{11} [MPa]	165000
	E_{22} & E_{33} [MPa]	9300
	ν_{12} & ν_{13} [-]	0.35
	ν_{23} [-]	0.487
	G_{12} & G_{13} [MPa]	5080
	G_{23} [MPa]	3127.1
	α_{11} [μm/m°C]	0.6
	α_{22} & α_{33} [μm/m°C]	33
	ρ [g/cm^3]	1.5
	Ply thickness [mm]	0.13

Abaqus Assembly module. Here the nut and bolt (without a washer) are modeled as a single part because the movement between the bolt and nut is considered not significant. The entire model is meshed using C3D8R elements; an 8 noded 3-dimensional brick element with reduced integration. A finer mesh was used at the vicinity of the plate-hole region and for the countersunk bolt (Fig. 3).

All the three materials (CFRP, aluminium and steel) are modeled as linear elastic, as the focus of this study is to understand the different stages of the bolted joint response before the initiation of damage. In addition, damage is mostly associated to bearing and is reported to happen at high applied displacements [3]. CFRP is modeled as an orthotropic elastic material (along with the thermal expansion coefficients in three directions) and the plies are defined using the 'Composite Layup' feature in Abaqus/Standard [35]. Since the study focuses only on linear elastic part, basic linear elastic material constitutive laws from Abaqus [35] are used for the simulations.

The contact interaction is assigned at three regions: (a) between the carbon and the aluminium plates; (b) between the bolt shaft and the hole of the plates and (c) between the bottom plate and the nut (modeled along with the bolt). This is simulated using the surface-to-surface contact algorithm in Abaqus/Standard, as recommended in Abaqus documentation [35] for the current problem. This interaction accounts for the friction and sliding between the contact surfaces, in addition to a hard contact over-closure relation. The hard contact defines the contact pressure between the two surfaces as a function of the over-closure of these surfaces (also referred to as the interpenetration of the surfaces). A small sliding tracking approach is assigned such that even if the bodies undergo large motions, there will be relatively little sliding. In addition, Abaqus uses an extended version of Coulomb's friction model [35] which accounts for the friction at the contact surfaces. Finite clearances are included between the bolt and the plate hole.

We defined the whole simulation in three steps, namely:

(a) Bolt pre-tension. The first step consists of applying a pretension force to the bolt by employing the 'Bolt Load' feature in Abaqus/Standard [35]. The elements underlying the pretension section are adjusted by Abaqus to obtain the prescribed amount of clamping force in the bolt. Further, this adjustment of the element length can be fixed so that the preload is maintained in the subsequent steps and the bolt can act as a deformable part when other loads are encountered [35].

(b) Thermal. Once the bolt has been tightened, a thermal step is performed to simulate the change in the thermal conditions, ranging from a room temperature (25 °C) to high (90°C) or low temperatures (-55°C). This temperature variation can be performed using the 'Predetermined field' option in Abaqus, where the target temperature and a ramp amplitude are specified.

(c) Tensile. Longitudinal tensile displacement is applied to one side of the assembly to simulate the shear response of the joint. All the nodes at one edge of the assembly are selected and applied a displacement in the in plane direction, while constraining the displacement in the other directions in order to have a pure in-plane loading. At the same time, nodes on the other edge are fixed.

Figure 2 presents the boundary conditions and applied load for the preload and tensile step for the SLS joint. During the bolt preload step, both the ends of the joint are clamped completely. During the thermal step, the same boundary condition as in the case of preload step is used. For the tensile loading, displacement is applied to all the nodes at one edge, while the other edge is still clamped. The force is obtained by summing all the reaction forces from the clamped joint end nodes.

In the bolt pre-tension and thermal steps, one of the options is to constrain all the degrees of freedom at one edge and leave the other free. This, however, lead to unfavorable out-of-plane movements. Hence, both ends of the assembly are constrained in all the degrees of freedom to simulate the bolt

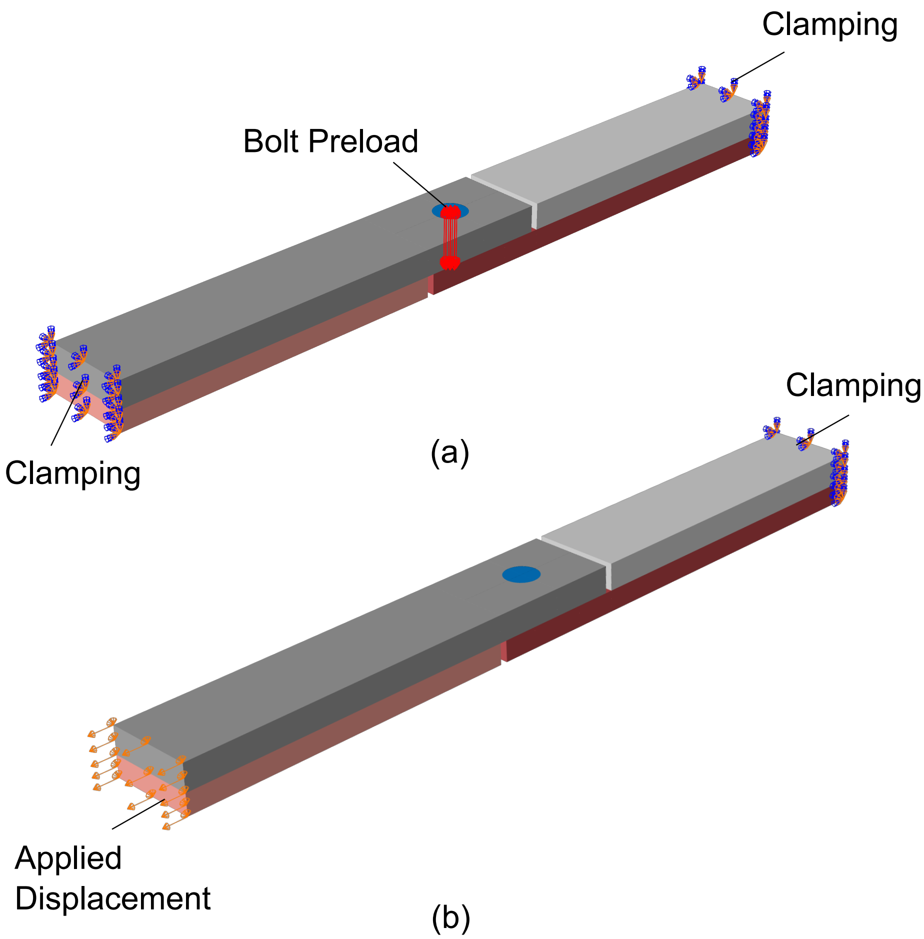

Figure 2: Load and boundary conditions detailed for (a) bolt preload and (b) tensile step.

preload and the temperature variation. In the tensile step, longitudinal displacement is applied to one side of the assembly, while the other end is constrained.

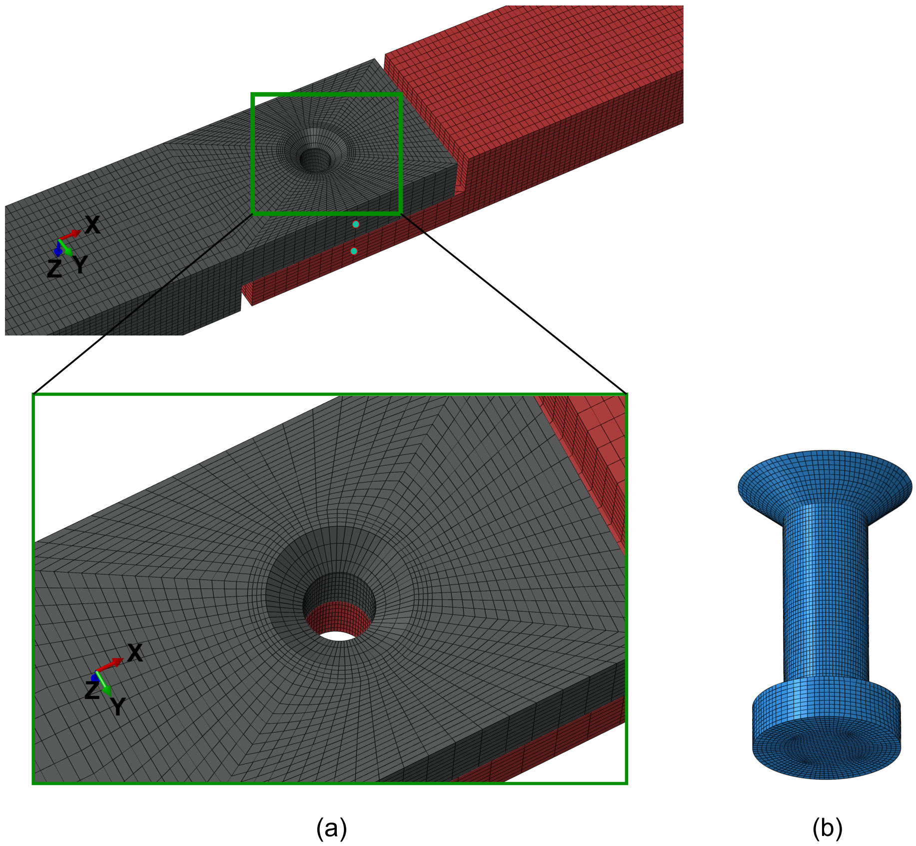

Figure 3: Details of the mesh discretization at the (a) bolt-hole region of the composite aluminium overlap region and (b) the countersunk fastener. (The top image also illustrates the extensometer locations (circles filled in green) to virtually measure sliding between the plates)

2.2. Definition of parametric study

Table 2 defines the different parameters the parametric study considers to understand their effect on the joint response. Case A is taken as the baseline. Here, the parameters correspond to typical values from references: a friction coefficient of 0.3 is considered. The other values considered to study the influence of high and low friction on joint behavior are 0.6 and 0.15, respectively. A clamping force of 6000 N (equivalent to a torque of 3.4 Nm) is considered as the baseline (in accordance with ASTM standards [37]), whereas a 'hand-tight' torque of 0.5 Nm, equivalent to a clamping force of 750 N, is selected as the other value. The selected clamping forces also ensure that there is no yielding in the bolt under the applied torque.

Typical aerospace structures use a bolt-hole clearance (defined as the difference in the diameter between hole and bolt shaft) in between 50-150 μm ([13; 38]), and in this study the baseline is taken as 60 μm. In addition, a higher clearance of 200 μm is explored to study the effects out-of-tolerance cases have on the joint behavior. Further, the influence of varying the thickness of the aluminium plate (a common industrial practice used to optimize the assembly depending on the loads) is also studied. Apart from the baseline value of 6 mm, thinner (4 mm) and thicker (9 mm) aluminium plates were investigated. As a final parameter and the main focus of this study, the thermal conditions were varied from room temperature to a positive thermal jump of 65 (25^oC to 90^oC) or a negative one of 80 (25^oC to -55^oC).

Table 2: Definition of the parameters for each case study

Case	Friction coefficient (μ) (-)	Bolt clamping force (CF) (N)	Bolt-hole clearance (BC) (μm)	Aluminium thickness (t_{Al}) (mm)	Thermal gradient (ΔT) (^oC)
A (Baseline)	0.3	6000	60	6	0
B	0.15	6000	60	6	0
C	0.6	6000	60	6	0
D	0.15	750	60	6	0
E	0.3	750	60	6	0
F	0.3	6000	200	6	0
G	0.3	6000	60	4	0
H	0.3	6000	60	9	0
I	0.3	6000	60	6	-80
J	0.3	6000	60	6	+65

Table 3 summarizes how the comparison of several cases from Table 2 allows for the effect of each investigated parameter on the joint response to be discussed.

Table 3: Compared cases and their corresponding targeted effects

Cases compared	Effect studied
A, B, C	Friction coefficient
A, E and B, D	Bolt clamping force
A, F	Bolt-hole clearance
A, G, H	Aluminium thickness
A, I	Negative thermal
A, J	Positive thermal

3. Results and Discussion

3.1. Mechanical response of a bolted joint

Fig. 4 (a) presents the force-displacement response of the baseline case under tensile loading. Here the plotted displacement is the one that is applied to all the nodes of the joint end and the force represents the reaction force obtained from the nodes at the other joint end that is clamped. The main objective is to understand the different stiffness stages in the shear response of the bolted joint. The same figure also illustrates the evolution in the contact status between the two plates (in Fig. 4 (b)) and the bolt shaft region under contact with the plates (in Fig. 4 (c)). Contact status is studied using CSTATUS output provided by Abaqus [35], where we can identify if the surfaces are completely in contact or in contact but sliding or no longer in contact.

The joint response can be divided into different stiffness stages, namely Stage I (0-1), Stage II (1-3), and Stage III (3-5). Stage I records the highest stiffness out of all the stages and no sliding between the plates is recorded (as seen in Fig. 4 (b)). No relative movement between the plates signifies that the load is carried by friction, and the maximum load taken by friction is the product of the clamping force (6000 N) and the coefficient of friction (0.3), i.e., around 1800 N (as seen in 4 (a)). Stage II (1-3), characterized by the sliding of the plates, starts when the load transferred by friction is surpassed, and the stiffness of this stage is much lower than that of Stage I. The relative movement between the plates starts and the closed contact status created by the preload clamping force changes to sliding (Fig. 4 (b)). The sliding of the plates continues until the bolt shaft comes in contact with the hole of the plates, which marks the beginning of Stage III (3-5). Fig. 4 (c) represents the evolution in the area of contact between the bolt shaft and the plates. The stiffness of Stage III is lower than that of Stage I, and with increasing displacement applied, the contact area between the bolt shaft and the hole increases.

The 3D numerical model provides an understanding of the contribution of the different forces acting on the bolted joint make. Fig. 5 presents the different in-plane force components, friction and normal forces between the various parts of the joint, that add up to the total applied load. The total load of the joint in Stage I is completely dominated by the friction between the two plates, i.e., without any contribution from the other forces. At around 0.06 mm displacement, the plates start to slide (beginning of Stage II) and the contribution from the frictional force between the plates tends to stabilize without adding any more to the total load. During the sliding stage, when the plates start to slide, the friction force under the nut increases until the bolt comes in contact with the plate hole. At 0.15 mm of applied displacement, the bolt comes in contact with the hole to start Stage III, where the normal force exerted by the bolt on the plates increases. With increased applied displacement, the bolt undergoes more bending and this results in an increase in the normal force thereby contributing

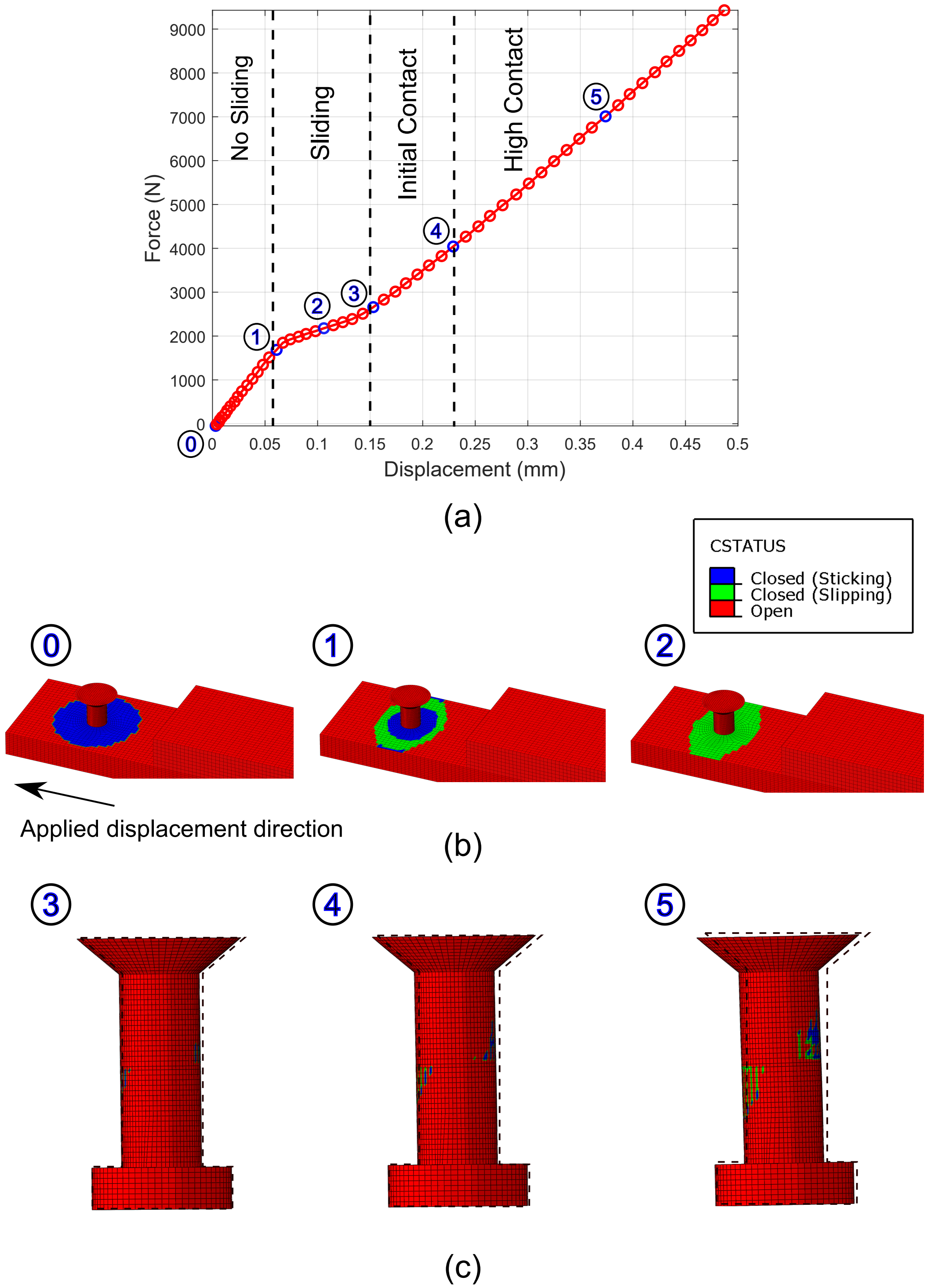

Figure 4: (a) Load-displacement response of the single lap shear bolted joint showing the different stiffness stages and (b) the evolution of the contact status in the aluminium rib and in the (c) countersunk fastener. (Note: The direction of the applied displacement is indicated in (b) and the initial position of the bolt with zero bending is marked using dashed lines in (c).)

to most of the total load on the joint (as seen in Fig. 5). With higher bending of the bolt, there is an increased contact area between the bolt and the plate holes, and the friction at the bolt-hole interface starts to contribute to the total load. Having said that, the frictional force component in the in-plane direction is much smaller when compared to the frictional force in the longitudinal axis of the bolt (out-of-plane component) [1]. The sum of these different force components adds up to the total applied load on the joint as in Fig. 5.

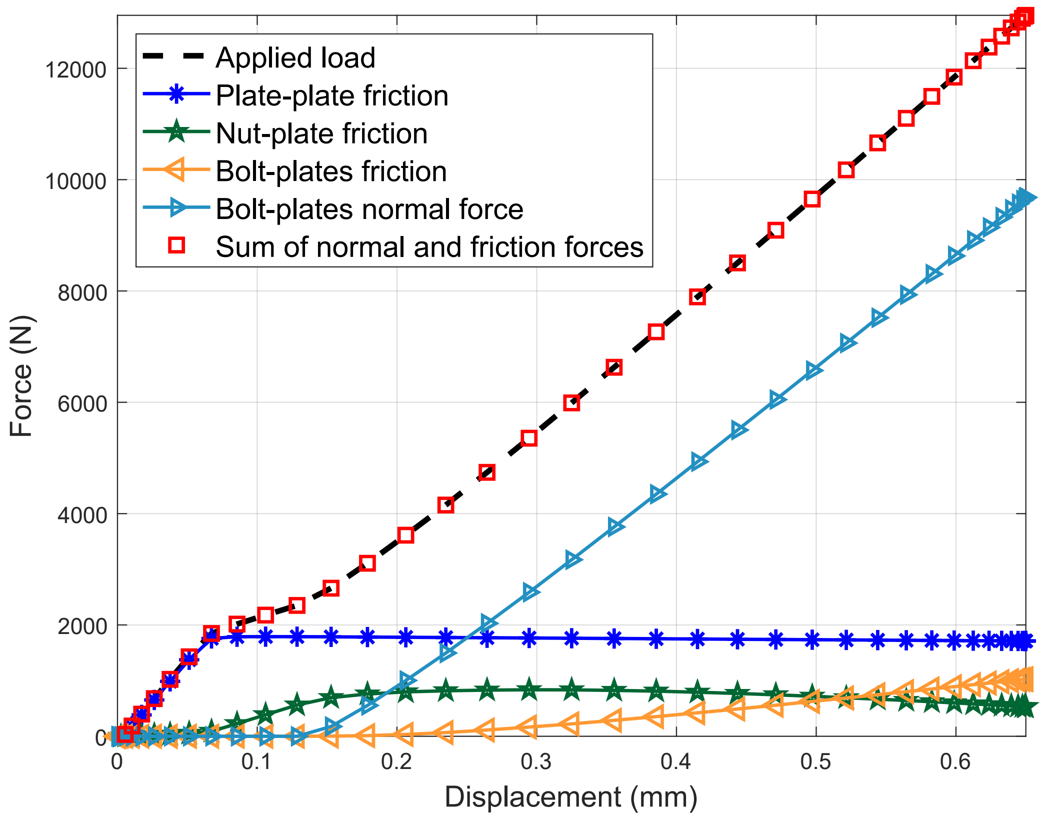

Figure 5: Different load contributions acting on the single lap shear bolted joint in the direction of the applied displacement for the tensile load step.

3.2. Parametric studies

Fig. 6 compares the variation in the bolted joint load-displacement response for the different friction coefficients. A higher coefficient of friction signifies that a higher load can be transferred through friction between the plates, before the onset of sliding. An increase in the friction values characterizes an extended Stage I response and a higher load carrying without any relative motion between the plates (3600 N, 1800 N and 900 N for μ=0.6, 0.3, 0.15, respectively).

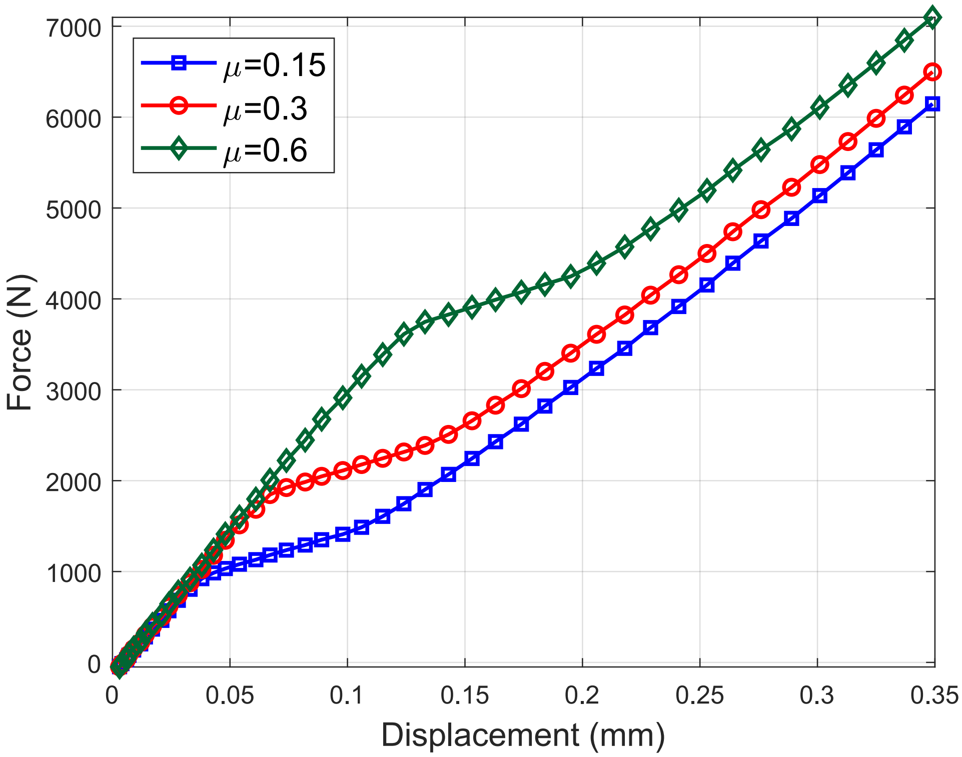

Figure 6: Effect of the coefficient of friction on the load displacement response of the joint behaviour with μ=0.15, 0.3 and 0.6.

A similar trend was seen in the joint response with the variation in the bolt clamping force. Fig. 7 (a) presents the response curves considering two clamping forces (for a standard friction value, 0.3) and similarly for Fig. 7 (b) but with a lower friction value (0.15). For a reduced bolt clamping force, the plate sliding (initiation of Stage II) occurs much earlier than that for an increased clamping force.

Fig. 8 compares the joint response for two different bolt-hole clearances. The change in clearance values does not affect the Stage I response, as this stage is completely dependent on the friction and bolt clamping values. Similarly, the initiation of Stage II is also unaltered with the change in clearance values, but the extension of Stage II is greatly influenced by the clearance. That is, the larger the clearance between the bolt and the hole, the greater the sliding between the plates, i.e., before the bolt comes in contact with the hole. Hence, a higher clearance value delays the onset of Stage III, or in other words, a delay in the load taken up by the bolt, as seen in Fig. 8. It is also important to note that there is a reduction (by around 16%) in the stiffness for Stage III for the higher clearance case in comparison to the lower clearance (Fig. 8). This is due to the difference in the contact area between the bolt and the hole with respect to the different clearance values. Fig. 9 (a) and (b) illustrate the development of the contact area within the hole of the aluminium plate for the lower and higher clearance values, respectively. The figures on the left and right indicate the contact area at the initial and final point of contact, respectively, between the bolt and the aluminium plate hole. For a higher bolt-hole clearance, the bolt undergoes further bending before making initial contact, i.e., a reduced area of contact as well as a reduced joint stiffness when compared to the lower clearance case.

Fig. 10 compares the force-displacement response of the joint for different aluminium plate thicknesses. The difference in the aluminium thicknesses results in different stiffnesses in Stage I. Compared to the baseline (6 mm), the thicker case (9 mm) has an 11% increase and the thinner (4 mm) with a 16% reduction in the stiffness in the stage I (Fig. 10).Apart from the differences in the stiffnesses, the maximum load attained by Stage I remains the same for all three cases as it depends solely on the friction and clamping force. The load transferred through friction is independent of the thickness of the plates. During stage II (sliding), no difference in the response is seen within the cases as the contribution to the total load is by the frictional force between the nut and the plate (as observed in Fig. 5). Likewise, the initiation of Stage III occurs at the same applied displacement for the different cases, but since stage III is characterized by the bolt-hole normal forces, the joint stiffnesses differ for each case, where the thicker aluminium plate coupon shows the highest joint stiffness.

3.3. Thermal effects

To study the thermal effects on the joint response, we compared the baseline case (with no thermal step) with two other cases, one with a positive thermal step and the other with a negative thermal step performed after the preload step and before the tension loading step. Fig. 11 presents the load-

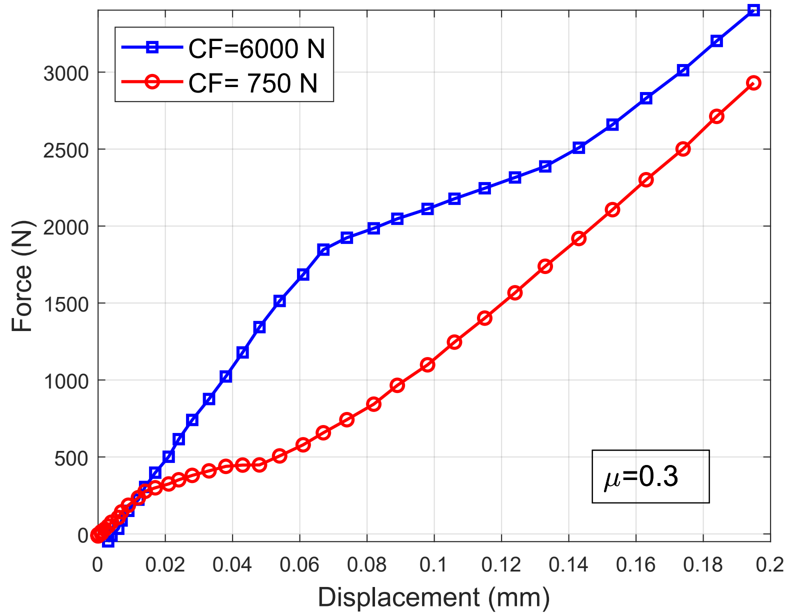

(a)

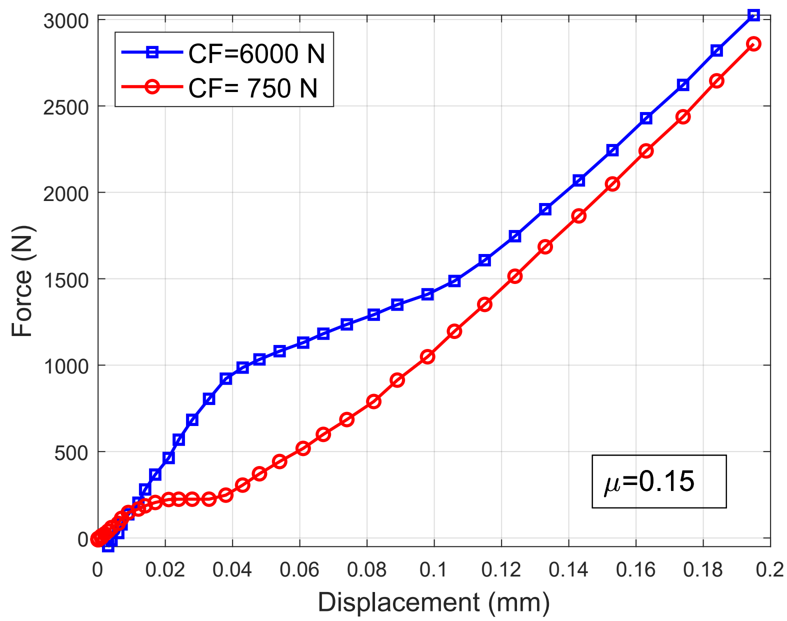

(b)

Figure 7: Effect of the bolt clamping force on the joint response for a friction coeffcient of (a) 0.3 and (b) 0.15.

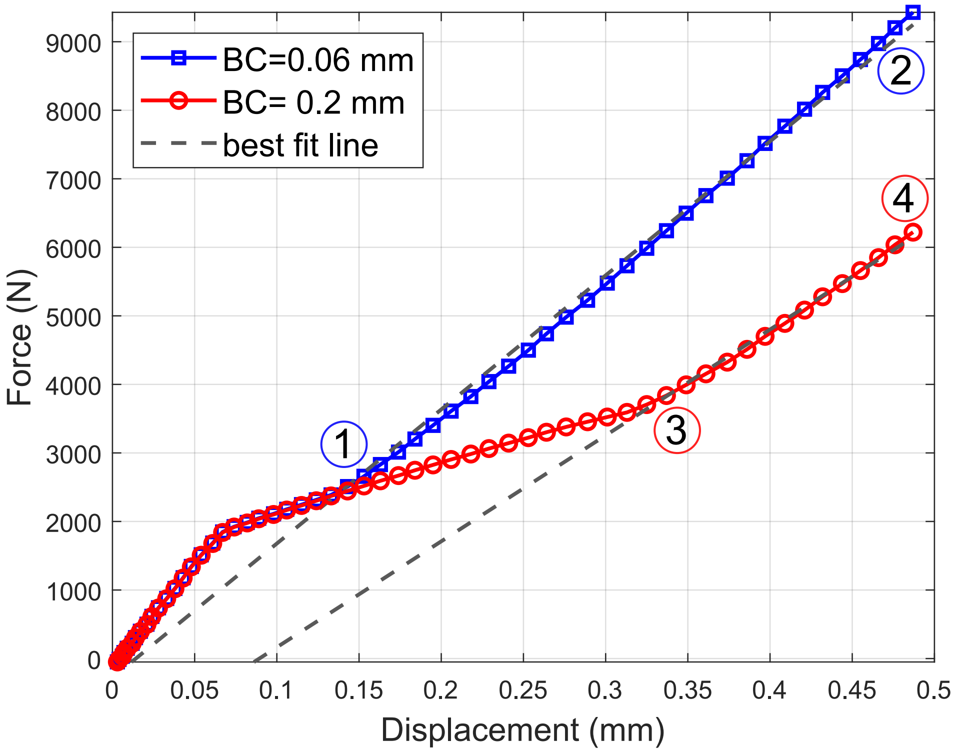

Figure 8: Effect of the bolt-hole clearance on the load displacement response of the joint behaviour. The reduction in the stiffness for Stage III for different bolt-hole clearance values is also shown. Points from 1-4 are used to demonstrate the evolution of contact area for different clearances in Fig. 9.

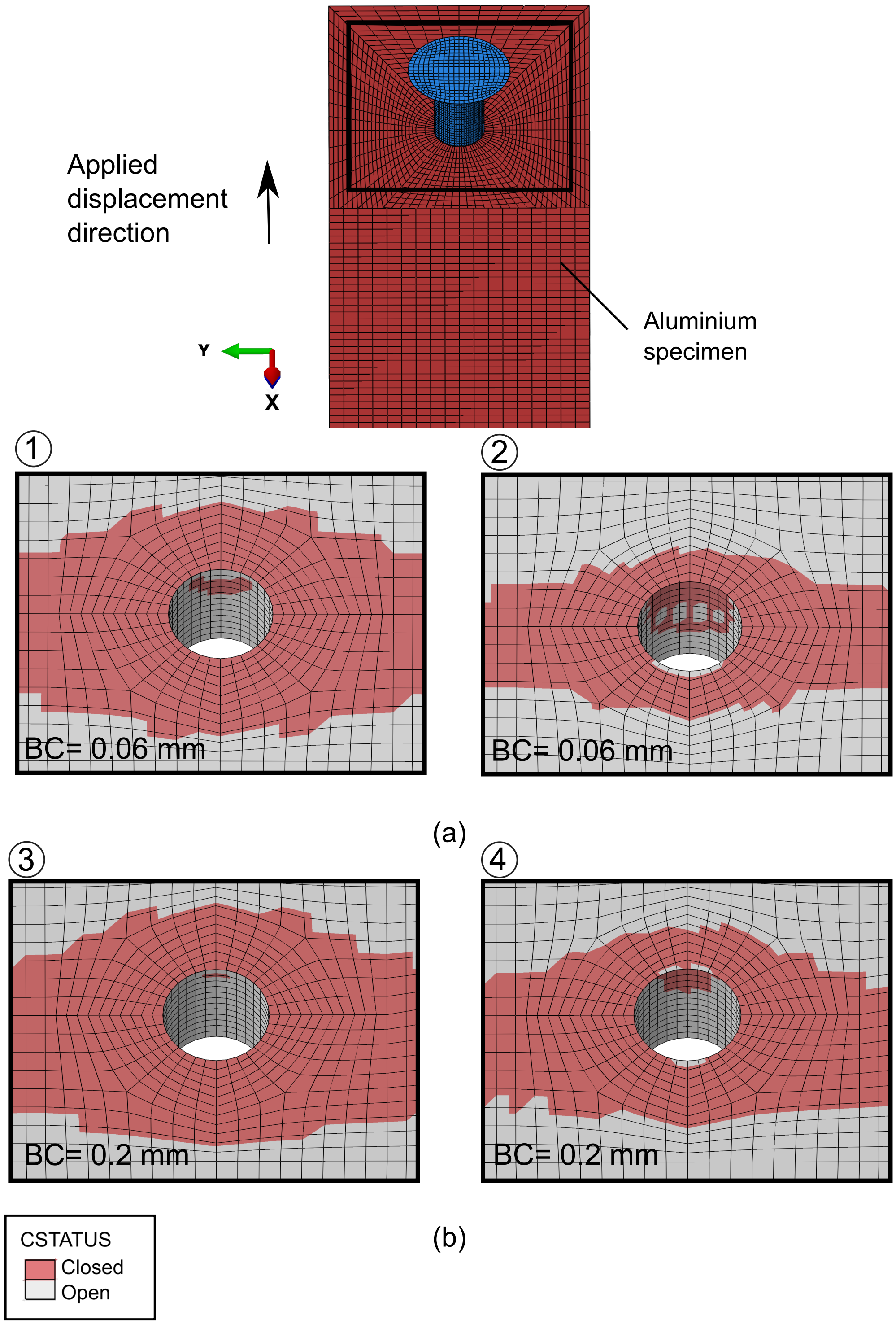

Figure 9: Evolution of the contact area at the hole of the aluminium plate for (a) lower and (b) higher bolt-hole clearance values. The left and right figures denote the inital and final point of contact, respectively, of the bolt with the hole. The top figure illustrates the region of study in the aluminium plate and also the direction of the applied displacement.

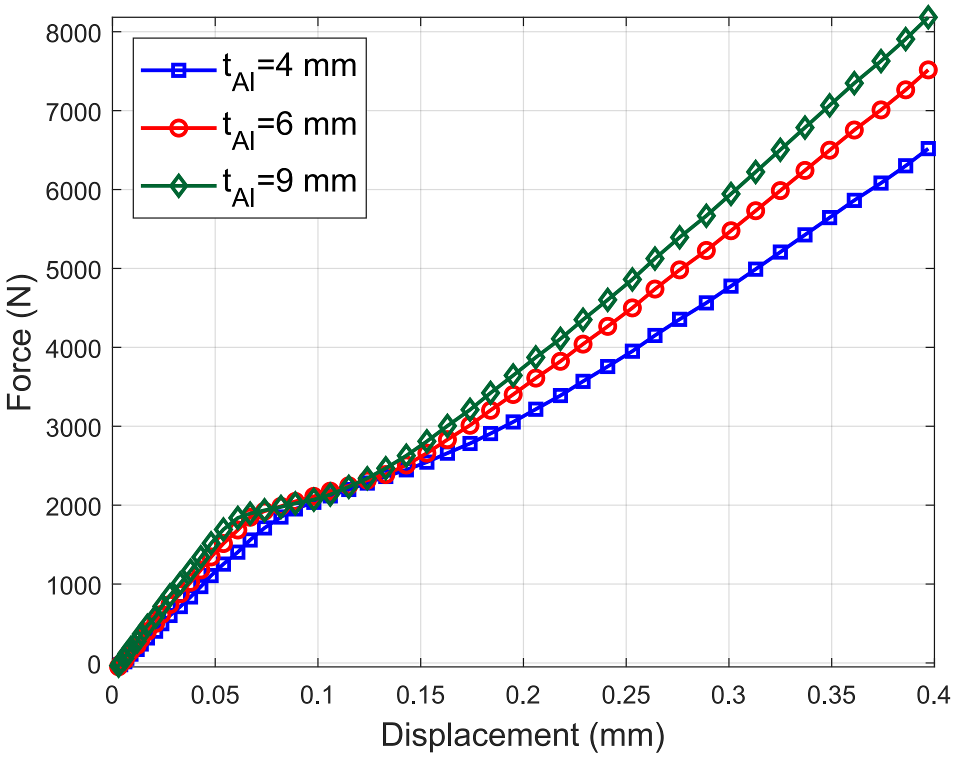

Figure 10: Effect of the thickness of the aluminium plate on the load displacement response of the joint behaviour with t_{Al}=4, 6 and 9 mm.

displacement response of the joint for the above-mentioned three cases. In the same figure, points A to C and A' to C' are also representing, respectively, the beginning and the end of the tensile step for all the three cases. Using these points, Fig. 12 a, b, and c compare the development of the bolt contact area with the plate hole and bolt bending for the three cases. The response curve of the baseline is already explained above in Fig. 4. In Fig. 12, point A shows the status of the bolt before the tensile step, and similarly point A' for the end of the tension step. Note that in this figure, the dashed black lines denote the initial bolt position to perceive the bolt's bending due to the thermal step.

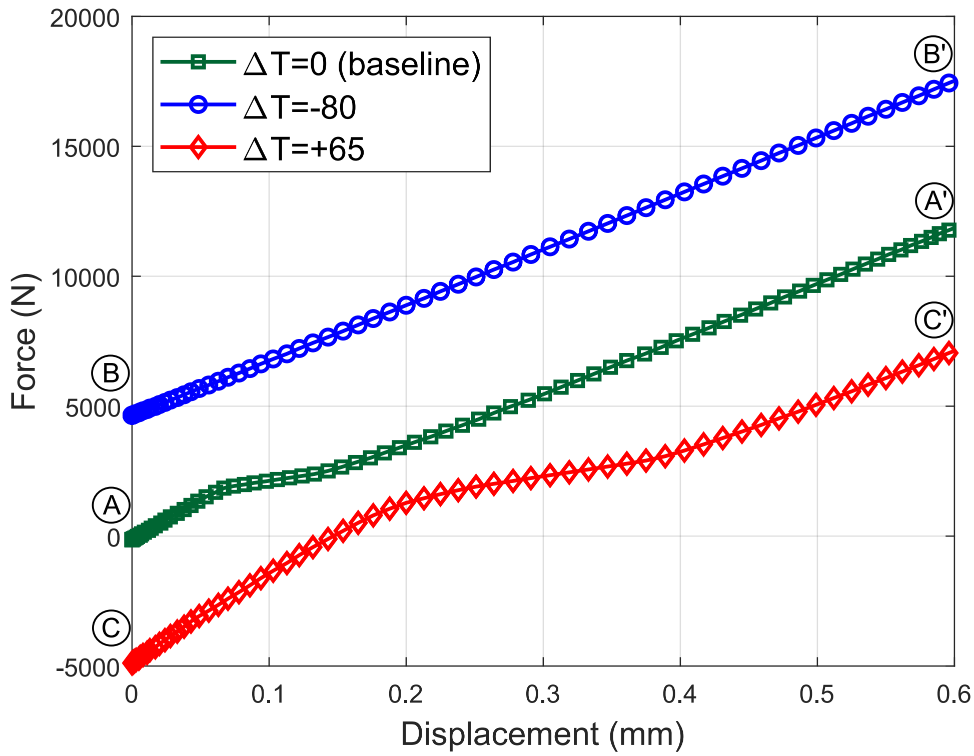

Figure 11: Comparing the load-displacement response of the baseline (without thermal step) with the cases including a positive and negative thermal step.

For the baseline, the bolt remains straight before the tensile step; as shown in Fig. 12 (a) in A. At the end of the tensile loading, the bolt bends in the counter clockwise direction (in the direction of the applied displacement) and we observe high contact of the bolt shaft with the holes (point A' in Fig. 12). In the case of the negative thermal step prior to the tensile loading, there is a tensile residual force of 5000 N at the end of the joint where the displacement is applied. This is due to the fact that during a negative thermal case, the whole joint contracts, and since the assembly is clamped at the ends, there is a positive reaction force at the joint end. The curve for the negative case, unlike the other cases, exhibits a single stage stiffness curve from the beginning to the end of the loading (Fig.

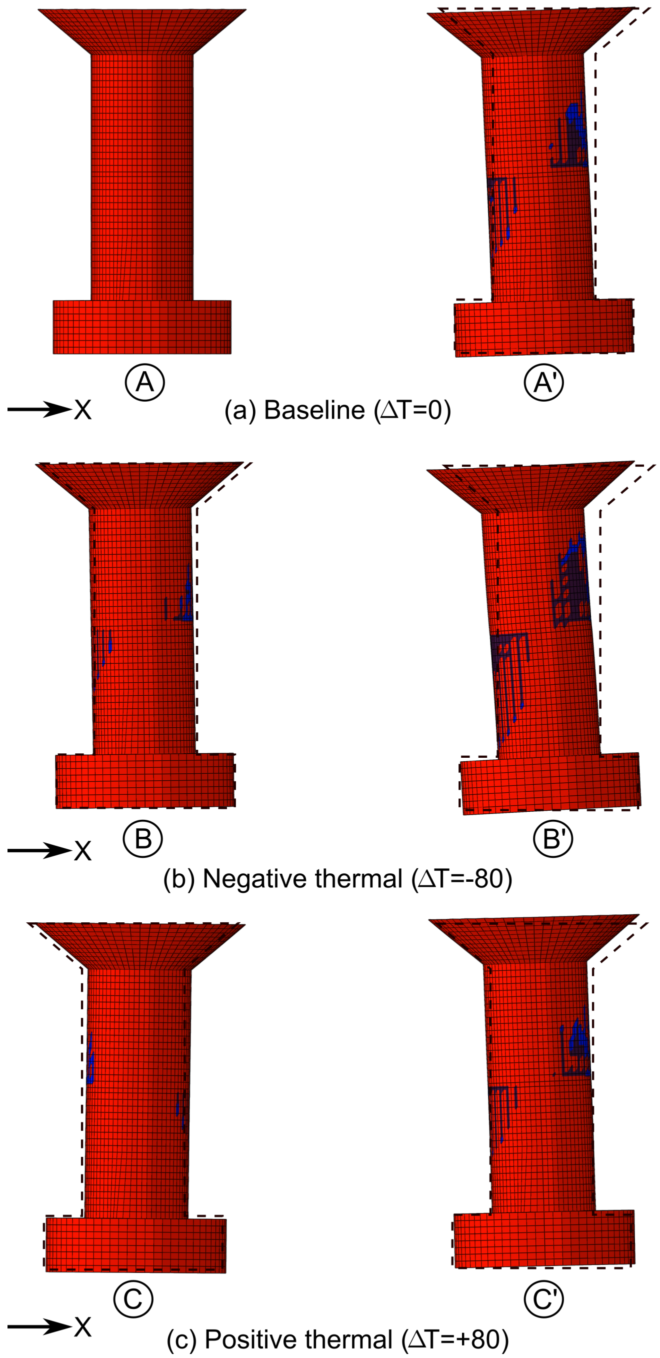

Figure 12: Development of contact area and bolt bending during the tensile loading, where the images on the left and right denote before and after tensile loading. Note that the displacement is applied in the negative X direction and the initial position of the bolt with zero bending is shown using dashed lines.

11). This is explained in the Fig. 12 as, due to negative thermal step, the aluminium at the bottom contracts more than the CFRP and the steel bolt, leading to the bolt bending in the counter clockwise direction. Hence, at the end of the thermal step, the bolt shaft is already in contact (for the given bolt-hole clearance value) as seen at point B. Further on during the tension step, the displacement is applied to the joint in the negative X direction, the bolt rotates further in this direction, thus creating a greater contact with the plate hole as seen at point B'. Thus, the single stiffness stage seen with the negative case in Fig. 11 is the joint stiffness when the bolt shaft is in contact with the hole. In addition, note that for all the above presented curves, the high magnitude of load is not realistic, as while considering damage, the final failure might have happened before reaching these high load levels.

A reverse phenomenon is noticed for the positive thermal case, as at the end of the thermal step, the joint expands and creates a compressive reaction force at the joint end (as in Fig. 11). Contrary to the negative thermal, the joint expands due to the positive thermal jump and the aluminium plate expands more than the CFRP and steel, leading to the bolt bending in the clockwise direction as seen in Fig. 12 (c) at point C. During tensile loading (applied in the negative X direction), the bolt bends back in the counter clockwise direction as seen in C' in Fig. 12. This is observed in the force-displacement response in Fig. 11 for the positive thermal case with three stiffness stages, where the first one refers to the joint stiffness when the bolt is in contact with the plates (as in C in Fig. 12). With applied displacement, the bolt rotates back to its initial position and gradually looses contact with the plate hole. In the second stage, the bolt is no longer in contact with the hole, hence the low stiffness in this stage. Further, with increased loading, the bolt swings to the direction of applied displacement and makes contact with the plate hole (point C' in Fig. 12), leading to the third stage in the curve.

Fig. 13 (a) presents the evolution of the bolt clamping force during the steps considered for the baseline (without thermal step), and the cases with positive and negative thermal steps included. Fig. 13 (b) shows the contact status between the plates at different time frames of the thermal load. During preload, the bolt undergoes tension to clamp the plates together. As seen in Fig. 13 (a), at the end of the preload step, the bolt force reaches the pre-defined value of 6000 N. A circular sticking contact region between the CFRP-aluminium interface demonstrates the clamping of the plates (Fig. 13 (b)).

During the negative thermal step, the plates contract more than than the steel bolt in the thickness direction, leading to a reduction in the bolt clamping force by around 40% when compared to the initial preload value. This loosening of the bolt is critical as it reduces the further load carrying capability of the joint [2]. Conversely, the positive thermal case induces a higher expansion in the plates compared to the bolt, thereby leading to an increase in the bolt clamping force by around 20%. A positive thermal case poses the threat of over-stressed bolts and possibilities of surpassing the yield stress of the bolt material. We observe sliding in both thermal cases (at step time 1.5 s in Fig. 13 (b)), but there is a clear difference in the contact profile and area between the negative and positive cases. At the end of the thermal step, the positive thermal still holds a uniform contact zone around the bolt, whereas the contraction of the plates in negative thermal step has caused a reduction in the contact zone (at step time 2.0 s in Fig. 13 (b)).

Further on during tensile loading, both thermal cases caused a reduction in the clamping force of the bolt, due to the shear sliding of the plates. In particular, the negative thermal case is more critical as the clamping force of the bolt is reduced to around 1000 N (compared to 6000 N and 3500 N, respectively, at the end of the preload and thermal steps) after the tensile loading. The drastic reduction in the bolt's clamping force when compared to the baseline case, demonstrates the effect that a negative thermal load can have on a torqued bolt.

Fig. 14 presents the relative shear sliding between the plates for both thermal cases. This was calculated from the relative difference in the in-plane displacements from the two nodes. A maximum shear sliding of 0.2 mm was recorded for the negative thermal case, which is critical enough to counteract the bolt-hole clearance and initiate contact between the bolt and the plates during a temperature difference (as seen in Fig. 12 (b) and (c)). An increase in temperature induces joint expansion and at the overlapping region of the dissimilar materials (as in Fig. 3(a)), the aluminium plate displaces in the negative X direction and CFRP in the positive X direction. The higher thermal expansion coefficient of aluminium has resulted in a four-fold higher in-plane displacement value when compared to the CFRP plate. A similar trend is seen with the negative thermal case, but in the reverse. During tensile loading, both the plates displace towards the negative X direction (direction of the applied displacement). The CFRP plate displaces more as the tensile loading was applied at the CFRP side of the assembly.

3.4. Loading-Unloading-Reloading cycle

We simulated a loading, unloading and reloading loop on the baseline case to study the joint response and evolution of contact regions. Aircraft experience a similar scenario but obviously in a higher number of cycles. Fig. 15 (a) presents the load-displacement response of the bolted joint for a loading, unloading and reloading loop. The joint is loaded until a displacement of 0.35 mm and then unloaded completely to a zero displacement. Further, the joint is reloaded by applying a displacement until 0.5 mm. We have selected different points in the joint response to study the contact evolution at different regions in detail. Fig. 15 (b) presents the contact tracking for the plate interface and the countersunk fastener for all the selected points throughout the loop. Fig. 16 presents the contribution of all the different forces (frictional and bearing force) that sums up to the total force during the whole loading-unloading-reloading cycle.

We explain the scenario by detailing each point as following:

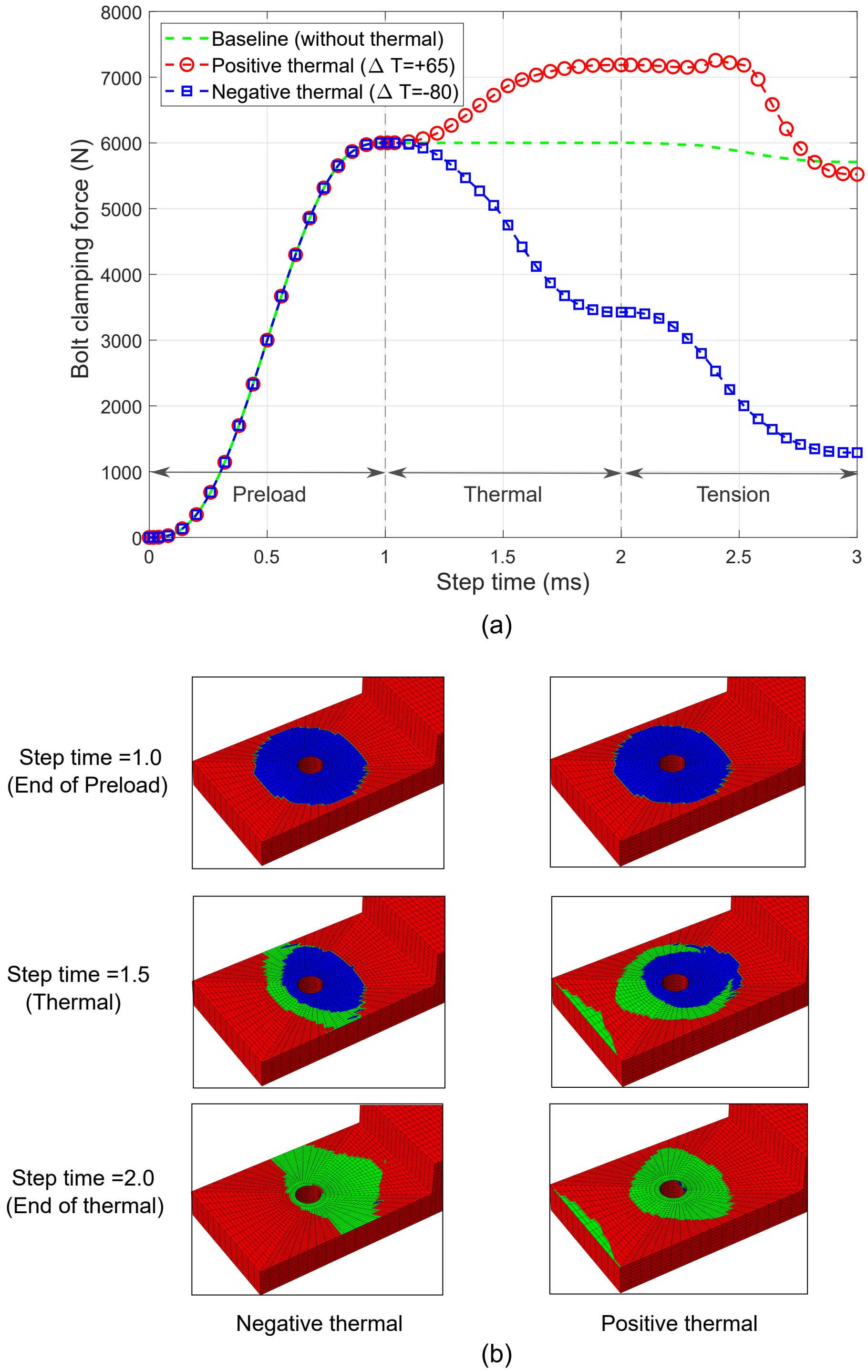

Figure 13: (a) Comparison of the evolution of bolt clamping force for the baseline (without thermal) and with thermal (positive and negative) cases. Note that the baseline does not have a thermal step and hence the value is kept constant. (b) Evolution of contact status at the plate interface during negative and positive thermal (note that the blue contour indicates closed (sticking) status and green indicates sliding).

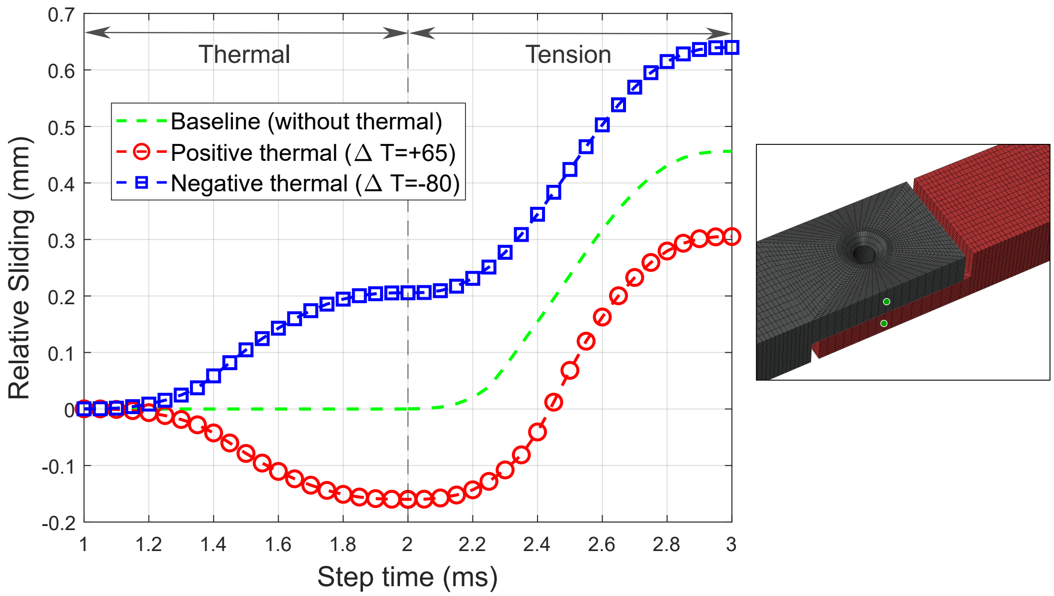

Figure 14: Shear sliding between the aluminium and CFRP plates for negative and positve thermal cases. (Note that the shear sliding was measured as the difference in the in-plane nodal displacements in the X direction measured at two nodes (marked in green circles) at the edge of each part at the center of the assembly, as shown in the sub-figure)

1: End of preload and beginning of tension step. Sticking contact zone at the plates' interface and at the aluminium plate-bolt nut interface.

2: End of stage I (characterized by friction) and beginning of stage II (sliding phase). At the end of stage I, the total reaction force equals the frictional force and hence the plates start to slide. The upper plate moves in the direction of the applied displacement (negative X direction) and the resulting frictional force acts in the positive X-axis (as shown in Fig. 15). Until point 2, total force is completely contributed by the plate-plate friction (see Fig. 16).

3: End of stage II and beginning of stage III, where there is complete sliding between the plates (all slipping region in Fig. 15 (b) point 3)) and initiation of contact between bolt shaft and the holes. Slight bolt rotation in the direction of applied displacement which leads to sliding and sticking at the plate-bolt nut interface. Plate-bolt bearing force starts to contribute to the total force as seen in Fig. 16.

4: Last point in the loading phase. Higher sliding between the plates and a reduced contact area compared to point 3. Higher contact between the bolt-shaft and holes and higher bolt rotation (compared to 3). As seen in Fig. 16, most of the contribution to the total force is from the plate-bolt bearing force due to the high contact and from the plate-plate friction force which remains constant from point 2 to point 4.

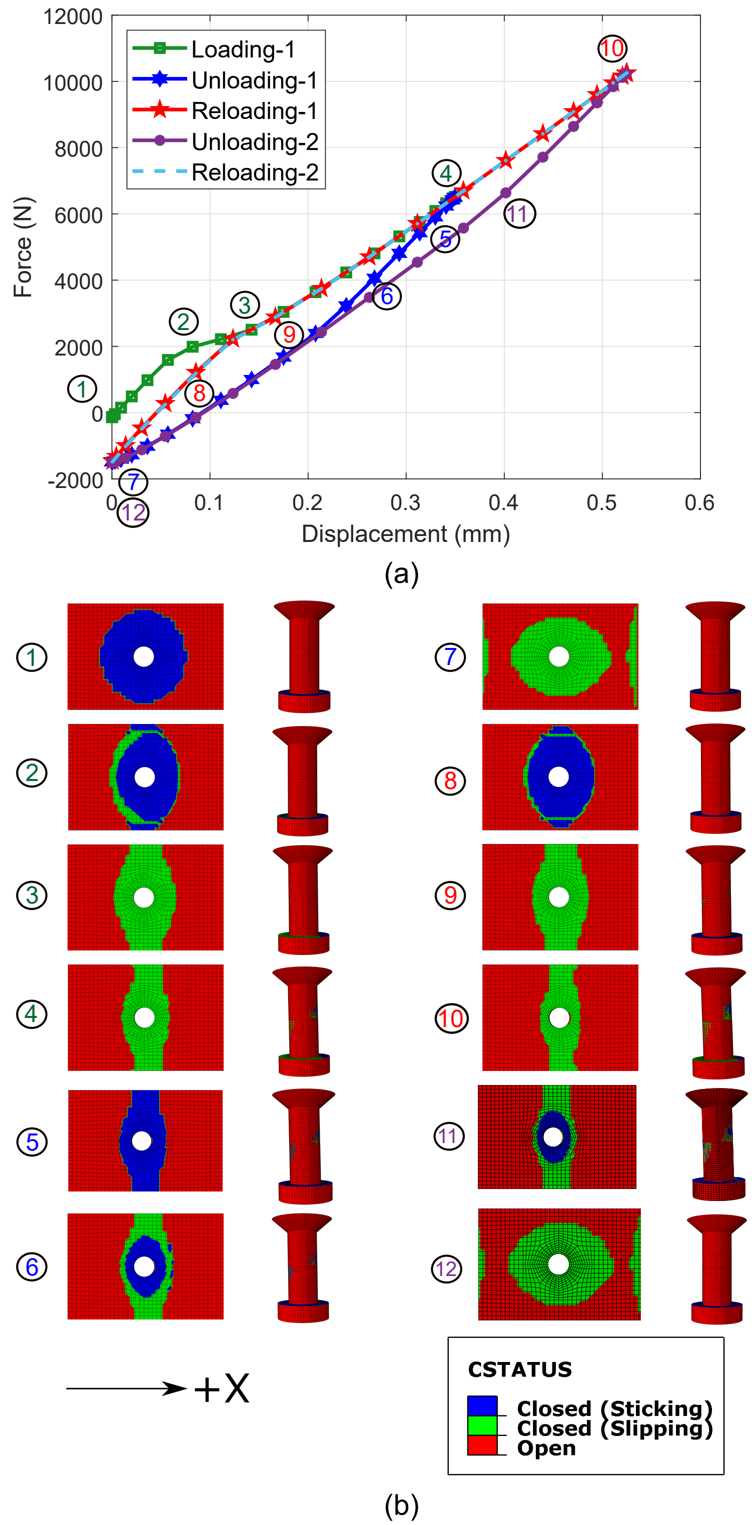

Figure 15: (a) Loading, unloading and reloading response of the single lap shear hybrid bolted joint and (b) Contact status at the aluminium plate and the countersunk bolt for selected points in the curve (note that the blue contour indicates closed (sticking) status and green indicates sliding)).

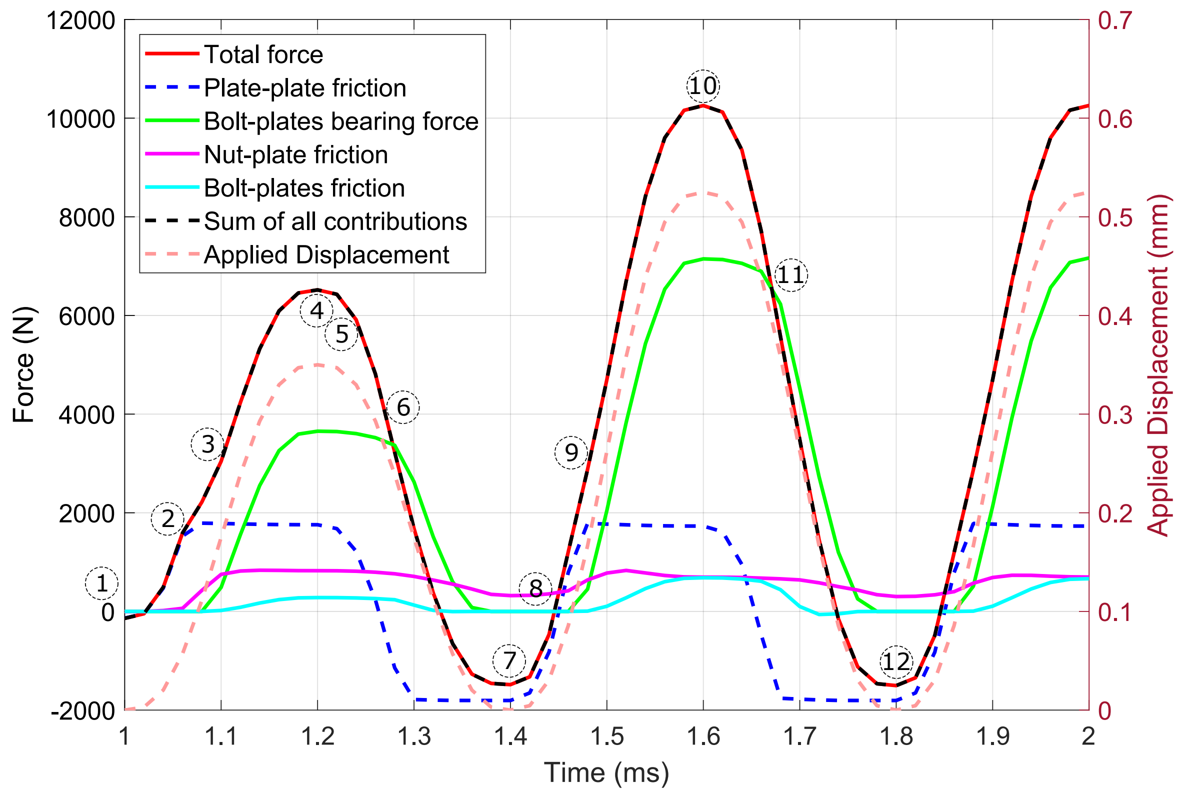

Figure 16: Evolution of total force (left Y axis) and displacement (right Y axis) with respect to time (X axis) during the whole loading-unloading and reloading cycle. Different force contributions (frictional forces and bearing forces) that sum up to the total force are also presented.

5: Beginning of the unloading phase. At this point of reversing the direction of the displacement, the displacement rate is null, and as a consequence, there is no sliding between the plates, shown by complete sticking in point 5 in Fig. 15 (b). At this point, the closed contact keeps contributing with a frictional force in the direction of the positive X-axis.

6: During unloading phase. When unloading starts (applied displacement direction is reversed), a fraction of the contact surface starts to slide, building a frictional force in the negative X-axis. At the same time, the closed area still contributes in the positive X direction. (Point 6 in Fig. 15 (b) shows both sticking and sliding regions in the contact area). Note that the bearing force between plate-hole and bolt shows a plateau during unloading (between t=1.2 to t=1.28 ms in Fig. 16), as a consequence of the contribution of the closed contact restricting the local displacement of the plate. This is understood as frictional hysteresis. During the transition from point 5 to 6, the fraction of sliding area increases while the closed contact decreases, hence the total frictional force grows in the negative X direction. At point 6 (t=1.275 ms, d=0.28 mm), the frictional force reaches zero as the contribution of the closed and sliding contact areas compensate with each other.

7: End of unloading phase. From point 6 to point 7, the sliding between the plates has increased, where the upper plate is moving to the positive X direction. Hence, a negative total force builds up as a consequence of the friction force (in the negative X direction), causing the observed compression total force at zero displacement (point 7 in Fig. 15 (b) or t=1.4 ms in Fig. 16). Bolt returns to the origin and hence no contact between the bolt and the plates, therefore a zero bearing force at point 7 (Fig. 16).

8: First point of reloading phase. Transition from point 7 to 8 is similar to the transition from point 4 to 5 but in the other direction. Total force and the plate-plate frictional forces are almost zero as seen in Fig. 16.

9: Second point in the reloading phase. The reloading curve joins the loading curve and similar response to point 3 in loading phase. Initiation of contact between bolt shaft and holes.

10: Highest displacement applied, extensive sliding and reduced contact surface between the plates. High contact of the bolt shaft and high bolt rotation. Close to complete slipping at the plate-bolt nut interface.

11: Point at the end of the first stage of unloading-2, where the friction force acts in the opposite direction (as explained in point 6).

12: Point of zero displacement in the second unloading loop. Same compressive total force as in point 7. At zero displacements, the total force is contributed solely by the plate-plate friction (in the negative X direction). The plate-plate frictional force remains the same at the end of each unloading stage, as it depends on the bolt preload which is retained to the initial preload value at the end of each unloading cycle. (see Fig. 16).

This study addressed the preliminary understanding towards the behaviour of a bolted joint with dissimilar materials under thermal and mechanical loads. With the key findings from this coupon level study, the next step in the framework of this project is to move to the sub-component level where we simulate the thermal response of a wing box sub component made of a single aluminium rib bolted to CFRP skin and spars using countersunk fasteners. Further, the ultimate objective is to model and simulate an entire hybrid wing box comprising of four different materials, to study the deformations arising from the thermal jumps.

4. Conclusion

In the quest to reduce weight, aircraft industries are combining metallic and lightweight carbon components in their primary structures. Aircraft structures with such hybrid joints, where the plates are made of dissimilar materials that expand differently with temperature, have shown signs of damage at the joint due to over stress and different responses at extreme temperatures. Hence, in this study, using a detailed 3D finite element model, we investigated the response of a hybrid bolted joint under thermal and mechanical loads. We simulated a single lap shear composite-aluminium joint with countersunk fastener using bolt preload, thermal jump and static tensile loading steps. Under mechanical tensile load, the joint response exhibits different stiffness stages characterized as 'No sliding', 'Sliding' and 'Contact'. Out of the different joint parameters studied, bolt-hole clearance exhibits a high influence in the sliding stage and determines the contact area between the hole and the plate. A higher out-of-tolerance clearance can impose a reduction in the joint stiffness, by around 16%, and also increased bolt bending and contact area. The coefficient of friction and bolt clamping force parameters only influenced the 'No sliding' stage. Further, we presented how thermal loading can significantly vary the bolt preload (40% reduction and 18% increase in bolt preload under negative and positive thermal conditions, respectively). In addition, a tensile load followed by a negative thermal step reduced the bolt preload by 85% compared to a baseline case with no thermal change. This drastic change can lead to bolt loosening (negative thermal) or over-stressed bolts (positive thermal), leading to a reduction in the load carrying capacity of the joint.

Acknowledgments

This work has been accomplished within the framework of an ongoing EU H2020 Clean Sky 2 Project INNOHYBOX (Innovative solutions for metallic ribs or fittings introduced in a composite box to optimally deal with thermo-mechanical effects). This project has received funding from the Clean Sky 2 Joint Undertaking (JU) under grant agreement No. 785433. The JU receives support from the European Union's Horizon 2020 research and innovation programme and the Clean Sky 2 JU members other than the Union.

Data Availability

The raw/processed data required to reproduce these findings cannot be shared at this time due to legal or ethical reasons.

References

[1] P. E. Irving, C. Soutis, Polymer composites in the aerospace industry, Woodhead Publishing, 2019.

[2] J. Bickford, An introduction to the design and behavior of bolted joints, revised and expanded (2018).

[3] C. Stocchi, P. Robinson, S. Pinho, A detailed finite element investigation of composite bolted joints with countersunk fasteners, Composites Part A: applied science and manufacturing 52 (2013) 143–150.

[4] L. Liu, J. Zhang, K. Chen, H. Wang, M. Liu, Experimental and numerical analysis of the mechanical behavior of composite-to-titanium bolted joints with liquid shim, Aerospace Science and Technology 100 (49) (2016) 167–172.

[5] EASA, Notification of a proposal to issue an airworthiness directive: Wing rib feet modification (2013).

[6] Airbus A380 wing flaw undetected for a decade, https://www.reuters.com/article/uk-airbus-a380/airbus-a380-wing-flaw-undetected-for-a-decade-iduslne84o00j20120525.

[7] C.-D. Coman, D. M. Constantinescu, Temperature effects on joint strength and failure modes of hybrid aluminum–composite countersunk bolted joints, Proceedings of the Institution of Mechanical Engineers, Part L: Journal of Materials: Design and Applications (2019) 1464420719837299.

[8] N. Hirano, Y. Takao, W.-X. Wang, Effects of temperature on the bearing strength of cf/epoxy pinned joints, Journal of composite materials 41 (3) (2007) 335–351.

[9] P. Camanho, S. R. Hallett, Composite joints and connections: principles, modelling and testing (2011).

[10] B. Vieille, J. Aucher, L. Taleb, Influence of temperature on the behavior of carbon fiber fabrics reinforced pps laminates, Materials Science and Engineering: A 517 (1-2) (2009) 51–60.

[11] J. Hu, K. Zhang, H. Cheng, Z. Qi, An experimental investigation on interfacial behavior and preload response of composite bolted interference-fit joints under assembly and thermal conditions, Aerospace Science and Technology (2020) 105917.

[12] T. Benhaddou, C. Chirol, A. Daidie, J. Guillot, P. Stephan, J.-B. Tuery, Pre-tensioning effect on fatigue life of bolted shear joints, Aerospace Science and Technology 36 (2014) 36–43.

[13] M. McCarthy, V. Lawlor, W. Stanley, C. McCarthy, Bolt-hole clearance effects and strength criteria in single-bolt, single-lap, composite bolted joints, Composites science and technology 62 (10-11) (2002) 1415–1431.

[14] B. Egan, C. T. McCarthy, M. A. McCarthy, R. Frizzell, Stress analysis of single-bolt, single-lap, countersunk composite joints with variable bolt-hole clearance, Composite Structures 94 (3) (2012) 1038–1051.

[15] F. Pierron, F. Cerisier, M. Grediac, A numerical and experimental study of woven composite pin-joints, Journal of Composite materials 34 (12) (2000) 1028–1054.

[16] M. McCarthy, C. McCarthy, V. Lawlor, W. Stanley, Three-dimensional finite element analysis of single-bolt, single-lap composite bolted joints: part i—model development and validation, Composite structures 71 (2) (2005) 140–158.

[17] C. McCarthy, M. McCarthy, Three-dimensional finite element analysis of single-bolt, single-lap composite bolted joints: Part ii—-effects of bolt-hole clearance, Composite Structures 71 (2) (2005) 159–175.

[18] D. Croccolo, M. De Agostinis, N. Vincenzi, Failure analysis of bolted joints: Effect of friction coefficients in torque–preloading relationship, Engineering Failure Analysis 18 (1) (2011) 364–373.

[19] Y. Xiao, W.-X. Wang, Y. Takao, T. Ishikawa, The effective friction coefficient of a laminate composite, and analysis of pin-loaded plates, Journal of composite materials 34 (1) (2000) 69–87.

[20] J. Schön, Coefficient of friction and wear of a carbon fiber epoxy matrix composite, Wear 257 (3-4) (2004) 395–407.

[21] R. Oskouei, T. Chakherlou, Reduction in clamping force due to applied longitudinal load to aerospace structural bolted plates, Aerospace Science and Technology 13 (6) (2009) 325–330.

[22] J. Lv, Y. Xiao, Y. Xue, Time–temperature-dependent response and analysis of preload relaxation in bolted composite joints, Journal of Reinforced Plastics and Composites 37 (7) (2018) 460–474.

[23] B. Montagne, F. Lachaud, E. Paroissien, D. Martini, F. Congourdeau, Failure analysis of single lap composite laminate bolted joints: comparison of experimental and numerical tests, Composite Structures 238 (2020) 111949.

[24] J. Lecomte, C. Bois, H. Wargnier, J.-C. Wahl, An analytical model for the prediction of load distribution in multi-bolt composite joints including hole-location errors, Composite Structures 117 (2014) 354–361.

[25] A. Olmedo, C. Santiuste, E. Barbero, An analytical model for the secondary bending prediction in single-lap composite bolted-joints, Composite Structures 111 (2014) 354–361.

[26] G. Scarselli, E. Castorini, F. Panella, R. Nobile, A. Maffezzoli, Structural behaviour modelling of bolted joints in composite laminates subjected to cyclic loading, Aerospace Science and Technology 43 (2015) 89–95.

[27] C. Hühne, A.-K. Zerbst, G. Kuhlmann, C. Steenbock, R. Rolfes, Progressive damage analysis of composite bolted joints with liquid shim layers using constant and continuous degradation models, Composite Structures 92 (2) (2010) 189–200.

[28] F. Zhuang, A. Arteiro, C. Furtado, P. Chen, P. P. Camanho, Mesoscale modelling of damage in single-and double-shear composite bolted joints, Composite Structures 226 (2019) 111210.

[29] F. Liu, W. Yao, L. Zhao, H. Wu, X. Zhang, J. Zhang, An improved 2d finite element model for bolt load distribution analysis of composite multi-bolt single-lap joints, Composite Structures 253 (2020) 112770.

[30] Z. Zhang, Y. Xiao, Y. Xie, Z. Su, Effects of contact between rough surfaces on the dynamic responses of bolted composite joints: Multiscale modeling and numerical simulation, Composite Structures 211 (2019) 13–23.

[31] Y. Zhou, Y. Xiao, Y. He, Z. Zhang, A detailed finite element analysis of composite bolted joint dynamics with multiscale modeling of contacts between rough surfaces, Composite Structures 236 (2020) 111874.

[32] Y. Xie, Y. Xiao, J. Lv, Z. Zhang, Y. Zhou, Y. Xue, Influence of creep on preload relaxation of bolted composite joints: Modeling and numerical simulation, Composite Structures 245 (2020) 112332.

[33] Z. Zhang, Y. Xiao, Y. Liu, Z. Su, A quantitative investigation on vibration durability of viscoelastic relaxation in bolted composite joints, Journal of Composite Materials 50 (29) (2016) 4041–4056.

[34] J. Kim, J.-C. Yoon, B.-S. Kang, Finite element analysis and modeling of structure with bolted joints, Applied mathematical modelling 31 (5) (2007) 895–911.

[35] V. ABAQUS User Manual, 6.14, Providence RI, USA: DS SIMULIA Corp (2014).

[36] J. M. Guerrero Garcia, A. Sasikumar, J. Llobet, J. Costa, A computationally efficient methodology to simulate hybrid bolted joints including thermal effects, Under review (2021).

[37] ASTM standard D 5961/D 5961M-96, standard test method for bearing response of polymer matrix composite laminates (1996).

[38] A. J. DiNicola, S. C. Fantle, Bearing strength behavior of clearance-fit fastener holes in toughened graphite/epoxy laminates, Eleventh Volume: Composite Materials—Testing and Design (1993).